Spiral Spin State in High-Temperature Copper-Oxide Superconductors: Evidence from Neutron Scattering Measurements

Per-Anker Lindgård*

Materials Research Department, Risø National Laboratory, 4000 Roskilde, Denmark

(Received 1 April 2005; published 15 November 2005)

An effective spiral spin phase ground state provides a new paradigm for the high-temperature superconducting cuprates. It accounts for the recent neutron scattering observations of spin excitations regarding both the energy dispersion and the intensities, including the "universal" rotation by 45° around the resonance energy $E_{\rm res}$. The intensity has a 2D character even in a single twin crystal. The value of $E_{\rm res}$ is related to the nesting properties of the Fermi surface. The excitations above $E_{\rm res}$ are shown to be due to in-plane spin fluctuations, a testable difference from the stripe model. The form of the exchange interaction function reveals the effects of the Fermi surface, and the unique shape predicts large quantum spin fluctuations in the ground state.

DOI: 10.1103/PhysRevLett.95.217001 PACS numbers: 74.72.−h, 74.20.−z, 74.25.Ha, 75.40.Gb

Understanding magnetic behavior is considered to be of fundamental importance for finding the mechanism [1] of high-temperature superconductivity (HTS), but several problems have emerged. A number of new neutron scattering studies [2–6] have determined the complete dispersion relations for several copper oxides of the HTS family. A remarkable universality has been revealed. An interpretation of the data [3] has been proposed in terms of two spin ladder stripes in equally populated twin domains. The stripe phase is a colinear, sinusoidal antiferromagnetic structure of the Cu^{2+} $S = \frac{1}{2}$ spins, separated by nonmagnetic stripes, Fig. 1(a). However, the details [7] (static, dynamic, nematic, etc.) are still debated, and several spin sites are not accounted for. Furthermore, the experiments [4] on an assembly of single-twinned crystals directly contradict the assumed 1D character. The stripes phase is, in addition, shown to be inconsistent with the latest detailed measurements and analysis [6]. An alternative paradigm is needed—and will be provided here.

The neutron data [2–6], obtained at the current experimental limits, reveal the most detailed information available on the spatial and temporal properties of the cuprates. The measured dispersion relation shows a low-energy "dome" and an inverted high-energy "dome" meeting at the resonance energy $E_{\rm res}$; see Ref. [3]. It is important to understand the implications. Here we shall take the most simplified picture, using the model Hamiltonian: $H = \Sigma_{\boldsymbol{q}} J(\boldsymbol{q}) \boldsymbol{S}_{\boldsymbol{q}} \cdot \boldsymbol{S}_{-\boldsymbol{q}} + H_{\rm an}$ with exchange interaction between localized spins, plus anisotropies. We shall determine the effective $J(\boldsymbol{q})$ and $H_{\rm an}$ in which all possible effects of doping and of quantum spin fluctuations are included.

First, consider the excitations for the LSCO family: $La_{2-x}(Sr, Ba)_xCuO_4$. La_2CuO_4 has long-range, antiferromagnetic order[8,9] with ordering vector $\boldsymbol{Q} = (\frac{1}{2}\,\frac{1}{2}\,0)$ r.l.u.. The excitation spectrum is well described by the above Hamiltonian, and with a very large 2D nearest neighbor superexchange [1,10] interaction [8] $J_1 = 146$ meV, which determines the magnetic energy scale. The spin directions are confined to the CuO_2 ab plane by an anisotropy due to quantum spin fluctuations [11] and/or exchange anisotropy [12,13].

In the doped systems, a fraction x of the Cu^{2+} ions are changed to nonmagnetic sites [singlets [14]]—introduced by the randomly placed, and immobile Sr^{2+} ions (or Ba^{2+} and O^{2-} in YBCO). The magnetic (short-range or long-range) order becomes incommensurate with scattering peaks at $\boldsymbol{Q}^{\pm}{}_h = \boldsymbol{Q}_{\rm AF} \pm \boldsymbol{\delta}$, $\boldsymbol{\delta} = (\delta 00)$, $\delta = x$ for $x < 1/8$. The doping further gives rise to a weak orthorhombic distortion of the ab plane, leading to twinning. This is unlikely to produce the significant uniaxial anisotropy needed for stabilizing the sinusoidal order, Fig. 1(a). Hence, we shall assume the fourfold symmetry to remain dominant, and that the twinning is capable only of selecting the ordering vector: i.e., $\boldsymbol{Q}^{\pm}{}_h$ in the a twins and $\boldsymbol{Q}^{\pm}{}_k = \boldsymbol{Q}_{\rm AF} \pm (0\delta 0)$ in the b twins, but does so without changing the basic interactions. The selection of a particular magnetic order and the distortion are coupled [4,15]. In general this will give rise also to an incommensurate lattice modulation. For incommensurate sinusoidal order, the linear excitation spectrum is complicated with an infinite Cantor set of energy gaps [16]. Here we shall investigate the more natural and simpler spiral phase, Fig. 1(a).

For spiral order, the dispersion relation and neutron scattering intensity [17,18] are simply determined by two frequencies:

$$\begin{aligned} \boldsymbol{\omega}_c(\boldsymbol{q}) &= \frac{2}{\hbar}[A + B + J(\boldsymbol{Q}) - J(\boldsymbol{q})] \\ \boldsymbol{\omega}_{a,b}(\boldsymbol{q}) &= \frac{2}{\hbar}\left[B + J(\boldsymbol{Q}) - \frac{J(\boldsymbol{Q}+\boldsymbol{q}) + J(\boldsymbol{Q}-\boldsymbol{q})}{2}\right] \end{aligned} \tag{1}$$

for oscillations in the c direction, and within the ab plane ($\hbar$ is Planck's constant divided by 2π, $\boldsymbol{Q} = \boldsymbol{Q}^{\pm}{}_h$). We have included a planar anisotropy term A and an in-plane anisotropy term B. The dispersion relation is given by

$$E(\boldsymbol{q}) = \hbar\sqrt{\boldsymbol{\omega}_{a,b}(\boldsymbol{q})\boldsymbol{\omega}_c(\boldsymbol{q})}. \tag{2}$$

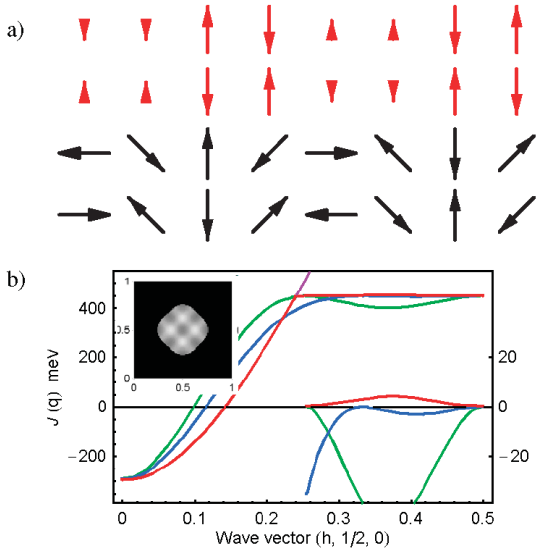

FIG. 1 (color). (a) Fractions of the discussed spin structures in the ab plane for $\delta = 1/8$. In black, the proposed spiral structure, with equal length spins on all sites. In red, the sinusoidal, uniaxial ordering. Note the variable spin lengths, which reduce the average magnetic energy by a factor two [22]. In the spin ladder "stripe" model [3] the small moments are even neglected, and hence 3 out of 4 spins are not accounted for. (b) The exchange interaction function, $J(\boldsymbol{q})$, which can generate the spiral order. The constructed $J(\boldsymbol{q})$ (red) compared with nearest neighbor functions having a plateau around $\boldsymbol{Q}_{\mathrm{AF}}$: Case (i) $J(\boldsymbol{q})^{\mathrm{i}}$, in green, with $J_2 = 0.655J_1$ and $J_3 = 0.311J_1$; (ii) $J(\boldsymbol{q})^{\mathrm{ii}}$, in blue, with $J_2 = 0.5J_1$ and $J_3 = 0.125J_1$. The detailed behavior of $J(\boldsymbol{q}) - J_{\mathrm{plateau}}$ magnified by a factor 10 is shown (curves around 0, right scale). The small 2D is a density plot of $J(\boldsymbol{q})$ in the full $(hk0)$ plane, showing the plateau and the added Fermi ridges along the $(\pm q, \pm q, 0)$ directions, giving peaks at both $\boldsymbol{Q}^{\pm}{}_h$ and $\boldsymbol{Q}^{\pm}{}_k$. There will only be significant neutron intensity within the plateau region, the detailed shape of which depends on the number of neighbor interactions. The thin, purple line is the extension of the J_1 cosine function.

The neutrons measure the c fluctuations at $\boldsymbol{q} = \boldsymbol{\kappa} + \boldsymbol{\tau}$, where $\boldsymbol{\kappa}$ is the momentum transfer, and $\boldsymbol{\tau}$ a reciprocal lattice vector. The intensities are

$$I_c(\boldsymbol{q}) = C(1 - \boldsymbol{\kappa}_c^2)\sqrt{\frac{\boldsymbol{\omega}_{a,b}(\boldsymbol{q})}{\boldsymbol{\omega}_c(\boldsymbol{q})}}\,\boldsymbol{\delta}(\boldsymbol{\kappa} + \boldsymbol{\tau} - \boldsymbol{q})$$
$$I_{a,b}(\boldsymbol{q}) = \frac{C}{2}(1 + \boldsymbol{\kappa}_c^2)\sqrt{\frac{\boldsymbol{\omega}_c(\boldsymbol{q})}{\boldsymbol{\omega}_{a,b}(\boldsymbol{q})}}\,\boldsymbol{\delta}(\boldsymbol{\kappa} + \boldsymbol{\tau} \pm \boldsymbol{Q} - \boldsymbol{q}), \tag{3}$$

where $\boldsymbol{\kappa}_c$ is the component of $\boldsymbol{\kappa}/\kappa$ along the c direction. C is a "constant" including a number of known effects; here $C \equiv 1$. The c-fluctuation branch has energy minima at $\boldsymbol{q} = \boldsymbol{Q}^{\pm}{}_h$ and a dome maximum at $\boldsymbol{q} = \boldsymbol{Q}_{\mathrm{AF}}$. The fluctuations within the ab plane follow the spiral rotation and are observed at $\boldsymbol{q} = \boldsymbol{\kappa} + \boldsymbol{\tau} \pm \boldsymbol{Q}$, with the intensity $I_{a,b}(\boldsymbol{q})$. These two branches also have minima at $\boldsymbol{Q}^{\pm}{}_h$, respectively, but rise to large values beyond $\boldsymbol{Q}_{\mathrm{AF}}$. Hence, near $\boldsymbol{Q}_{\mathrm{AF}}$ they contribute exclusively to the upper dome [see Ref. [3]], while all contribute to the lower one. The spectrum remains, but is broadened in $\boldsymbol{q}$ space in the presence of random doping, and if the magnetic order is short ranged [19].

What is the effect of doping on $J(\boldsymbol{q})$? Doping extends the electron wave functions, causing larger and longer-range neighbor interactions. Instead of using a model with different neighbor interactions, we shall, as a new method, construct a suitable 2D $J(\boldsymbol{q})$ directly in reciprocal space using an analogy to the Cu metal [20]. We assume that effective, localized spins remain, but they now further interact by polarization of a small nonlocalized part of the electrons, which determine a Fermi surface. The nesting features of this result in an increased electron susceptibility at the wave vectors $\boldsymbol{Q}^{\pm}{}_{h,k}$. The qualitative features of the measurements allow one to set up certain constraints:

(1) Ordering at $\boldsymbol{Q}^{\pm}{}_h$ demands that $J(\boldsymbol{Q}_{\mathrm{AF}} \pm \boldsymbol{\delta})$ is maximum.

(2) The "domes" meeting [3] at the resonance energy at $\boldsymbol{Q}_{\mathrm{AF}}$ requires that $J(\boldsymbol{Q}_{\mathrm{AF}}) = J(\boldsymbol{Q}_{\mathrm{AF}} \pm 2\boldsymbol{\delta})$.

(3) The accurate $\delta = x$ relation for $x < 1/8$ requires that $J(\boldsymbol{q})$ be extremely flat around $\boldsymbol{q} = \boldsymbol{Q}_{\mathrm{AF}}$ with a small x-dependent Fermi peak added.

In real space, H has the form: $H = \Sigma_{i,n} J_n \boldsymbol{S}_i \cdot \boldsymbol{S}_{i+n} + H_{\mathrm{an}}$; then $J(\boldsymbol{q}) = \Sigma_n J_n(\nu_{nh} + \nu_{nk}) + J_n{}'\nu_{nh}\nu_{nk}$, where $\boldsymbol{q} = (hk0)$, J_n is the interaction to neighbor group, n, along $(h00)$ and $(0k0)$, $J_n{}'$ are diagonal interactions, and $\nu_{nx} = \cos(2\pi nx)$. In the doped samples, numerous J_n and $J_n{}'$ constants are expected, if a Rudermann-Kittel-type interaction [20] is involved. The conditions (1)–(3) can be met approximately by introducing just two additional, smaller neighbor interactions: Case (i) $J(\boldsymbol{q})^{\mathrm{i}}$ with $J_2 = 0.655J_1$ and $J_3 = 0.311J_1$ yields a flat maximum with equal values at $\boldsymbol{Q}_{\mathrm{AF}}$ and $\boldsymbol{q} = \boldsymbol{Q}_{\mathrm{AF}} \pm 2\boldsymbol{\delta}$; an even flatter, but smaller region around $\boldsymbol{Q}_{\mathrm{AF}}$ may be obtained by introducing: Case (ii) $J(\boldsymbol{q})^{\mathrm{ii}}$ with $J_2 = 0.5J_1$ and $J_3 = 0.125J_1$. Neither function is sufficiently flat, however [see Fig. 1(b)], for the $\delta = x$ relation to be fulfilled precisely. To avoid introducing many parameters, we construct $J(\boldsymbol{q})$ in 2D using the functional form given by merely the J_1 cosine function $(\nu_{1h} + \nu_{1k})$, and make a plateau around $\boldsymbol{Q}_{\mathrm{AF}}$ by cutting off the top at the value at $\boldsymbol{Q}_{\mathrm{AF}} + 2\boldsymbol{\delta} + (0.01, 0, 0)$, yielding: $J(\boldsymbol{q})_{\mathrm{cut}} = J_{\mathrm{cut}}(\nu_{1h} + \nu_{1k})_{\mathrm{cut}}$. The small addition represents, effectively, a smoothing of the cutoff; introducing a proper Gaussian smoothing of the plateau edge does not alter our results significantly. On top of the plateau, we add the Fermi surface peaks. The Fermi surface has a diamond shape and the sharp nesting is perpendicular to this shape (giving an expected deviation around $\boldsymbol{Q}_{\mathrm{AF}}$ along the diagonal directions), whereas the $\boldsymbol{q}$ dependence along the diamond edges should be very broad. To simulate this we add 4 small ridges of Gaussian shape. This yields the total effective interaction function (apart from a constant, which is determined by $\Sigma_q J_q = 0$; it does not play a role in the dispersion relation or the intensities):

$$J(\boldsymbol{q}) = J_{\mathrm{cut}} + J_{\mathrm{Fermi}}[\exp\{-w(k - 1/2 + h - \boldsymbol{Q}^{\pm}{}_h)^2\} + \exp\{-w(k - 1/2 + h + \boldsymbol{Q}^{\pm}{}_h)^2\} + \{h \leftrightarrow k\}].$$

With this model it is possible to obtain a quantitative fit to all the neutron scattering data published on LSCO. For Ba substitution [3] with $x = 1/8$: $J_{\text{cut}} = 508$ meV and $J_{\text{Fermi}} = 2.8$ meV. This roughly corresponds to introducing further neighbor interactions $(J_1, J_2, J_3) = (195 \pm 15, 112 \mp 7, 41 \mp 15)$ meV: upper and lower values correspond to cases (i) and (ii) shown in Fig. 1(b), where the various $J(\boldsymbol{q})$ functions are compared [21]. The nearest neighbor interactions are both enhanced and of longer range in the doped case, which is not surprising because of the enhanced electron mobility (larger overlap). The Fermi peak is barely visible on top of the plateau in Fig. 1(b); the behavior of $J(\boldsymbol{q}) - J_{\text{plateau}}$ is amplified by a factor of 10, right scale. The width, w, is determined by the shape of the lower "dome." The small 2D inset shows a density plot of the plateau and the added Fermi ridges along the $(\pm q, \pm q, 0)$ directions. Hence, the important Fermi peak (the position of which depends linearly on x) has a small amplitude of 5.6 meV and is quite broad, FWHM = 0.125 r.l.u. $\sim \delta$ (determined by the shape of the lower dome). The maxima $(=2J_{\text{Fermi}})$ at intersections of the ridges cause the incommensurate ordering to occur, surprisingly, at a $\boldsymbol{\delta}$ along the $(h00)$ and $(0k0)$ directions. A very small anisotropy: $A = B = 0.03$ meV, can give rise to an energy gap of 6 meV, as observed in the superconducting state [5].

For a single twin domain, the predicted energy-integrated 2D intensity is shown on Fig. 2. The c fluctuations contribute with a strong peak (lower dome) in both the $(h00)$ and $(0k0)$ directions. The $J(\boldsymbol{q})$ plateau and the Fermi ridges are reflected in the nearly spherical high-intensity region. The in-plane fluctuations cause only intensity in the lens-shaped regions (consisting of fractions of the above shape around $\boldsymbol{Q}^{\pm}{}_h$). The in-plane ab fluctuations are solely responsible for the upper dome around $\boldsymbol{Q}_{\text{AF}}$, and the intensity in this energy range comes chiefly along the edges of the plateau in $J(\boldsymbol{q})$. Hence, the shape of the plateau is reflected in the details of the measured 2D intensity plots for constant, high-energy segments. Figure 3 shows a plot of the energy and the intensity for a section along $(h\tfrac{1}{2}0)$. Outwards from $\boldsymbol{Q}^{\pm}{}_h$ the branches are split, while being essentially degenerate in the lower dome; hence the dome is more intense. The intensity near $\boldsymbol{Q}^{\pm}{}_h$ is reduced owing to the small density of states, whereas the "resonance" peak arises because of the high density of states at $\boldsymbol{Q}_{\text{AF}}$. The resonance value, here $E_{\text{res}} = 55$ meV, measures the height of the Fermi peak: the square root of $2J_{\text{Fermi}} = J(\boldsymbol{Q}_h) - J(\boldsymbol{Q}_{\text{AF}})$ times essentially $2J_1$, or more precisely $J(\boldsymbol{Q}_{\text{AF}}) - J(\delta, 0, 0)$. The upper dome is given by the full range of $J(\boldsymbol{q})$ times contributions near the edge of the lenses.

The excitation spectrum for the spiral state resolves a large number of puzzles found experimentally [2–6]. For a detailed comparison, an accurate simulation of the experimental conditions is required. The intensity from energy segments identical to the measured ones are collected and then folded by a width function. The width (HWHM = 0.05 r.l.u.) primarily reflects the disorder due to the lack of long-range magnetic order, and secondly experimental resolution. The result is shown on Fig. 4. It demonstrates the remarkable 45° rotation of the pattern for the lower dome $E < E_{\text{res}}$ and the upper dome $E > E_{\text{res}}$. The intensity for the upper energies reflects the outer edges of the lenses—and thus can, depending on possible interactions to further neighbors, vary between box over ring to diamond shape. This is therefore not universal, contrary to the shift of symmetry between the lower and upper "dome," which is a property of the spiral state and the flat plateau.

The model also describes the YBCO ($YBa_2Cu_3O_{6+x}$) compounds [2,4,6], with the "universal" rotation of the intensity pattern below and above E_{res}. For $x = 0.6$: $E_{\text{res}} = 34$ meV and $\delta = 0.1$ r.l.u., and the plateau is smaller with a radius of about 2δ. The measured dispersion can be fitted

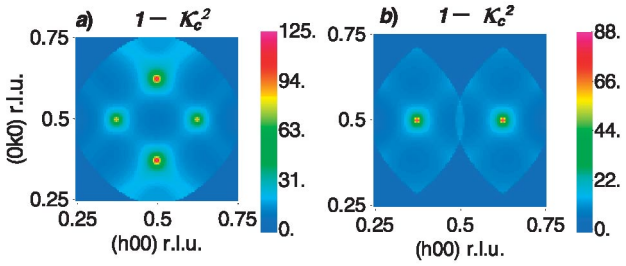

FIG. 2 (color). Density plot of the energy-integrated neutron intensity in the $(hk0)$ plane for a single a twin of LSCO, $x = 1/8$, with spiral ordering vector $\boldsymbol{Q}^{\pm}{}_h$. Panel (a) shows the contribution from the c fluctuations, which is to be multiplied by $(1 - \boldsymbol{\kappa}_c^2)$. Notice the strong intensity also at $\boldsymbol{Q}^{\pm}{}_k = \boldsymbol{Q}_{\text{AF}} \pm (0\delta 0)$. Panel (b) shows the sum of the in-plane ab fluctuations, which is to be multiplied by $(1 + \boldsymbol{\kappa}_c^2)$. These only peak at $\boldsymbol{Q}^{\pm}{}_h$. The observed intensity is the sum of all contributions.

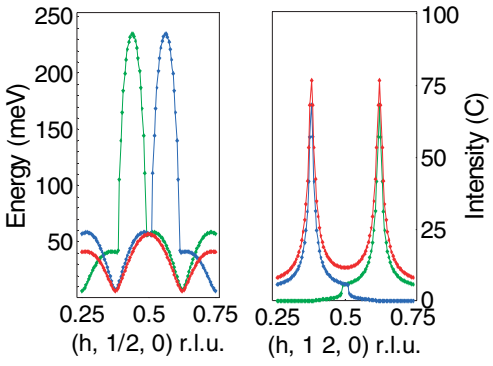

FIG. 3 (color). Excitation energy and intensity for long-range spiral structure with parameters as for $La_{2-x}Ba_xCuO_4$, $x = 1/8$. The red curve represents the c fluctuations, the green and blue curves the in-plane ab fluctuations. A comparison with the experimental dispersion curve can only be made after appropriate folding with the width function (see text). This widens the upper dome to about $\pm 2\delta$ in agreement with experiments [3]. Notice the branches are nearly degenerate for the lower "dome," but split going outwards, hence the dome will appear more intense.

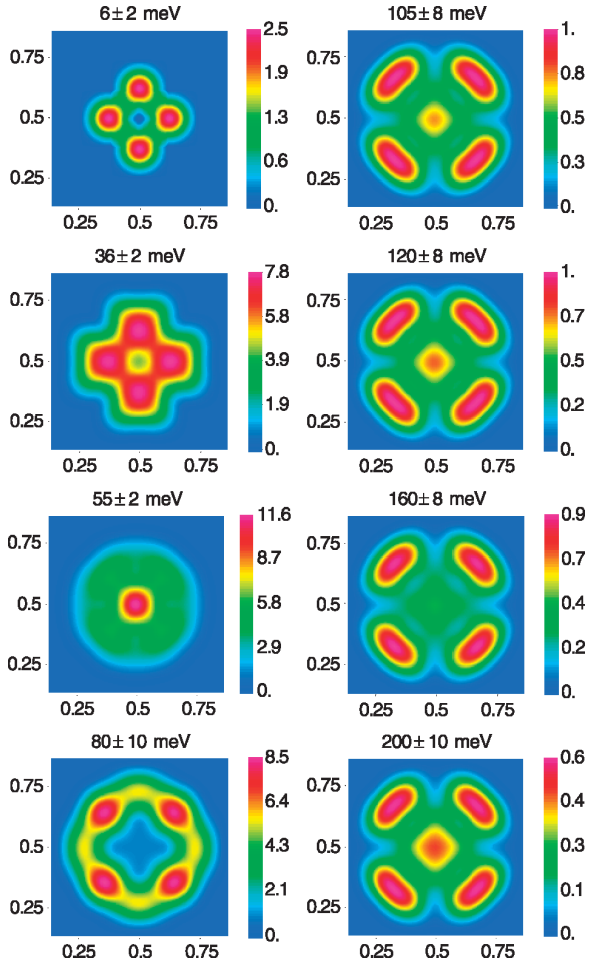

FIG. 4 (color). Density plots of the calculated intensity for $La_{2-x}Ba_xCuO_4$, $x = 1/8$, here symmetrized in the $(hk0)$ plane for equal a- and b-twin populations [notice the experimental data [3] are plotted in a 45° rotated coordinate system]. We have folded by a 2D Gaussian function in $\boldsymbol{q}$ space with a HWHM = 0.05 r.l.u. and added the c and ab fluctuations equally. Notice the maximum intensity occurs at the resonance peak at $E_{\rm res} = 55$ meV concentrated near $\boldsymbol{Q}_{\rm AF}$ as observed experimentally. The peaks rotate 45° around this energy as a consequence of the spiral order. $I_c(\boldsymbol{q})$ contributes for $E > E_{\rm res}$ with a weak ring at the outer edge of the plateau, Fig. 2(a).

with: $J_{\rm Fermi} = 1.4$ meV, FWHM $= \delta$, and $J_{\rm cut} = 216$ meV or $(J_1, J_2, J_3) = (135 \pm 10, 77 \mp 4, 28 \mp 10)$ meV. In a single twin sample we find significant 2D intensity from $I_c(\boldsymbol{q})$, Fig. 2(a), for $E < E_{\rm res}$ in agreement with the measurements [4].

In conclusion, we have shown that an effective spiral spin state provides a new paradigm on which to build theories of HT_c superconductivity. Neutron scattering measurements of the magnetic excitations in the superconducting cuprates can be both qualitatively and quantitatively understood in such terms. The spiral phase is the reason for the measured universal behavior—which is therefore not an indication of stripe order. The deduced form of the magnetic interaction function shows long-range couplings and contributions from a Fermi surface. The high-energy modes near $\boldsymbol{Q}_{\rm AF}$ are shown to originate from in-plane spin fluctuations—while out-of-plane fluctuations also contribute to the low-energy modes. This prediction (which has not been obtained in the stripe phase model) provides new evidence for resolving the high-temperature superconductivity puzzle, and can be verified by further neutron scattering investigations—even in twinned crystals. The "resonance" peak measures the size of the Fermi contribution, which is sensitive to the electronic ground state. The energy gap measures the anisotropy. This is presumably influenced by quantum fluctuations of the spins, which are predicted to be extremely large because of the plateau in $J(\boldsymbol{q})$. Hence the emerging picture is not in contradiction to the spin fluctuation models proposed by Anderson [1].

The author thanks N. H. Andersen, H. Rønnow, and T. Ziman for valuable comments. This work is supported by the Danish Technical Research Council under the Framework Programme on Superconductivity.

*Email address: P.A.Lindgard@Risoe.dk

[1] P. W. Anderson, P. A. Lee, M. Randeria, T. M. Rice, N. Trivedi, and F. Z. Zhang, J. Phys. Condens. Matter **16**, R755 (2004).
[2] S. M. Hayden, H. A. Mook, V. Dai, T. G. Perring, and F. Dogan, Nature (London) **429**, 531 (2004).
[3] J. M. Tranquada *et al.*, Nature (London) **429**, 534 (2004).
[4] V. Hinkov *et al.*, Nature (London) **430**, 650 (2004).
[5] N. B. Christensen *et al.*, Phys. Rev. Lett. **93**, 147002 (2004).
[6] C. Stock *et al.*, Phys. Rev. B **71**, 024522 (2005).
[7] V. J. Emery, S. A. Kivelson, and J. M. Tranquada, Proc. Natl. Acad. Sci. U.S.A. **96**, 8814 (1999).
[8] S. M. Hayden *et al.*, Phys. Rev. Lett. **67**, 3622 (1991).
[9] R. Coldea *et al.*, Phys. Rev. Lett. **86**, 5377 (2001).
[10] P. W. Anderson, Phys. Rev. **115**, 2 (1959).
[11] P.-A. Lindgård, Phys. Rev. Lett. **61**, 629 (1988).
[12] O. Entin-Wohlman, A. B. Harris, and A. Aharony, Phys. Rev. B **53**, 11 661 (1996).
[13] T. Yildirim, A. B. Harris, O. Entin-Wohlman, and A. Aharony, Phys. Rev. Lett. **73**, 2919 (1994).
[14] F. C. Zhang and T. M. Rice, Phys. Rev. B **37**, 3759 (1988).
[15] S. J. L. Billinge, M. Gutmann, and E. S. Bozin, Int. J. Mod. Phys. B **17**, 3640 (2003).
[16] T. Ziman and P.-A. Lindgård, Phys. Rev. B **33**, 1976 (1986).
[17] P.-A. Lindgård, A. Kowalska, and P. Laut, J. Phys. Chem. Solids **28**, 1357 (1967).
[18] B. I. Shraiman and E. D. Siggia, Phys. Rev. Lett. **62**, 1564 (1989).
[19] P.-A. Lindgård, Phys. Rev. B **27**, 2980 (1983).
[20] P.-A. Lindgård, X.-W. Wang, and B. N. Harmon, J. Magn. Magn. Mater. **54-57**, 1052 (1986).
[21] Fourier transforming the deduced $J(\boldsymbol{q})$ yields the corresponding interaction constants.
[22] P.-A. Lindgård, Phys. Rev. Lett. **78**, 4641 (1997).